Curved Membrane Mimics for Quantitative Probing of Protein-Membrane Interactions by Surface Plasmon Resonance

Alexander S. Malinick, Daniel D. Stuart, Alexander S. Lambert, and Quan Cheng*

Department of Chemistry
University of California, Riverside
CA 92521, USA

*Corresponding author: Quan Cheng

Tel: (951) 827-2702, Fax: (951) 827-4713

Email: quan.cheng@ucr.edu

Abstract:

A majority of biomimetic membranes used for current biophysical studies rely on planar structures, such as supported lipid bilayer (SLB) and self-assembled monolayers (SAM). While they have facilitated key information collection, the lack of curvature makes these models less effective for the investigation of curvature-dependent protein binding. Here we report the development and characterization of curved membrane mimics on a solid substrate with tunable curvature and ease in incorporation of cellular membrane components for study of proteinmembrane interactions. The curved membranes were generated with an underlayer lipid membrane composed of DGS-Ni-NTA and POPC lipids on the substrate, followed by attachment of histidine tagged cholera toxin (his-CT) as a capture layer. Lipid vesicles containing different compositions of gangliosides, including GA₁, GM₁, GT_{1b}, and GQ_{1b}, were anchored to the capture layer, providing fixation of the curved membranes with intact structures. Characterization of the curved membrane was accomplished with surface plasmon resonance (SPR), fluorescence recovery after photobleaching (FRAP), and nano tracking analysis (NTA). Further optimization of the interface was achieved through principal component analysis (PCA) to understand the effect of ganglioside type, percentage, and vesicle dimension on their interactions with proteins. In addition, Monte Carlo simulations were employed to predict the distribution of the gangliosides and interaction patterns with single point and multi-point binding models. This work provides a reliable approach to generate robust, component-tuning, and curved membranes for investigating protein interactions more pertinently than what traditional planar membrane offers.

Keywords: Surface plasmon resonance, curved membranes, gangliosides, protein interactions, principal component analysis

Introduction:

Cellular membranes encircle and reside within all cells, playing crucial roles in many cellular functions. Lipids, the backbone of cellular membranes, divide the line between extracellular and intracellular interactions and control the packaging and transportation of various biological components across and within cells. Various cellular functions such as cell division, endo- and exocytosis, organelle trafficking, and signal transduction rely on the composition, structure, and curvature of membranes to work properly. Because of their dynamic and integral roles, a great deal of research has focused on the development of membrane mimics to characterize and investigate the diverse and fundamental biophysical interactions. ³⁻⁶

To date, vast majority of membrane mimics have relied on the use of self-assembled monolayers (SAM) and supported lipid bilayers (SLB) to investigate these complex interactions.⁴ 6-12 While SAM and SLB are valuable models, especially as biomimetics, they have several drawbacks. Most notably is that both are planar surfaces, lacking in curvature or curvature tuning, which have led to misrepresentation when compared to the natural structure of cells and the interactions they attempt to mimic.⁶ Although much knowledge has been gained on how the composition of planar lipid membrane affect biophysical interactions, 3, 6, 12 it is becoming more evident that curvature needs to be taken into account in the studies. ¹³⁻¹⁵ SAMs and SLBs have been effective in the examination of many types of biological interactions, ^{7,8,16} however, a large portion of these interactions and their properties still remains less investigated and poorly understood, especially in regards to the interactions that require curvature. ^{13-15, 17, 18} Several methods have been developed to investigate the properties of these interactions using specific interfaces on biosensor's surface with surface functionalization. 13, 19-28 However, they are limited by a number of factors including the composition of the membrane, the degree of curvature, reproducibility, and the fluidity of the membrane. There is a compelling need for the development of new approaches that can reliably generate reproducible curved membranes through simple procedures for modification to be used in functional studies.

Curved membrane mimics are also important systems for structural recreation of unique environments essential to certain interactions as many biological entities, such as proteins, viruses, and cells, rely on membrane curvature for communication, transportation, and regulation. ^{15, 17, 18,}

²⁹ Varied degree of membrane curvature prove to be necessary to deciphering these interactions, ^{15,} ^{18, 30} and to yielding a deeper understanding of some disease-specific pathways. ^{15, 31, 32} Several complex diseases such as cancers, Alzheimer's, Parkinson's, Huntington's disease, multiple sclerosis, muscular dystrophy, and COVID-19 have been linked to protein interactions that rely on curved membranes. ^{15, 31, 33-35} Specifically, curvature sensing proteins, such as alpha synuclein and bridging integrator 1, have shown strong dependence of the binding properties to curved membranes. ^{15, 32, 36} Investigating these biophysical interactions may aid in the development of new therapeutics, drug delivery, and disease detection.

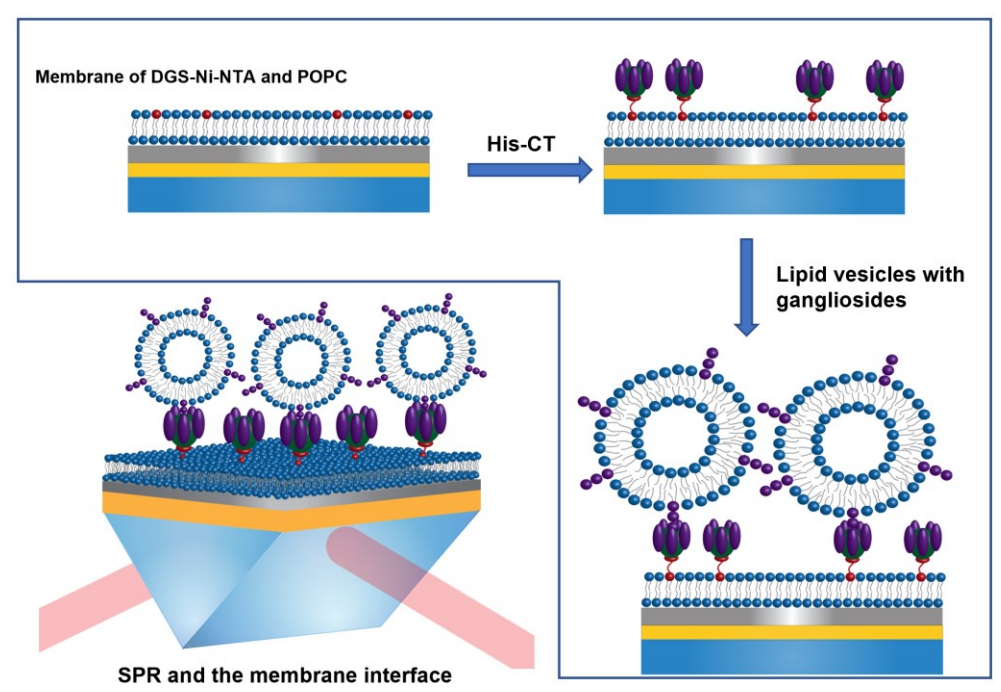


Figure 1. Schematic illustration to show the formation of a supported curved membrane with the capture protein and ganglioside-functionalized vesicles.

In this work, we report a method to steadily create a curved membrane interface with lipid vesicles for the study of curvature-dependent protein interactions with surface plasmon resonance (SPR) (Figure 1). The vesicles could be straightforwardly modified to incorporate various types of glycans and other membrane components, allowing one to control the composition and size of the curved membrane mimics with ease. Vesicle sizes between 30 nm to 200 nm were selected as this is the typical range for endosomes and exosomes, and represents the characteristic curvature that many proteins interact with. ^{17,33,37} Gangliosides were chosen as the primary membrane component as they are present in various highly curved membranes, such as the myelin sheath, ^{7,8,20,31} and a

range of 0.05 % to 5 % was used due to the biologically relevance.^{38, 39} Aside from characterizing the structural construction of the platform, we employed cholera toxin (CT) to study the interactions on the varied curvature and evaluate the interaction patterns towards a multi-point or single point binding mechanism through the effect of curvature.

EXPERIMENTAL METHODS:

Materials and Reagents:

Asialoganglioside GA₁ and tetrasialoganglioside GQ_{1b} were acquired from Sigma-Aldrich (St. Louis, MO). Monosialoganglioside GM₁ was purchased from Matreya (Pleasant Gap, PA). Trisialoganglioside GT_{1b} was obtained from Biosynth (Itsaca, II). 5B-sub-unit histidine tagged cholera toxins was purchased from Sigma-Aldrich (St. Louis, MO). 1,2-dioleoyl-sn-glycero-3-[(N-(5-amino-1-carboxypentyl)iminodiacetic acid)succinyl] (nickel salt) DGS-Ni-NTA, 1-palmitoyl-2-oleoyl-glycero-3-phosphocholine POPC, mini stainless steel extruder, 1,2-dipalmitoyl-sn-glycero-3-phosphoethanolamine-N-(7-nitro-2-1,3-benzoxadiazol-4-yl) (ammonium salt) NBD, and 30 nm, 100 nm, and 200 nm polycarbonate thin film membranes were all purchased from Avanti Polar Lipids (Alabaster, Al). Premium Plain BK-7 glass microscope slides and phosphate buffered saline (PBS) concentrate were purchased from Fisher Scientific (Pittsburgh, PA).

Lipid Vesicle Preparation:

Stocks of 5 mg/mL POPC and 5 mg/mL GA₁, GM₁, GT_{1b}, and GQ_{1b} were diluted in 1:9 methanol chloroform solution to the designated concentration and stored in a –80 °C freezer. Lipid vesicle formation was achieved by aliquoting the lipid stock solution into glass vials and drying under nitrogen to form a thin lipid film that was left to dry for 24 hours in a vacuum desiccator. The dried lipids were resuspended in 1× PBS (10 mM Na₂HPO₄, 1.8 mM KH₂PO₄, 137 mM NaCl, 2.7 mM KCl, pH 7.4) to a final concentration of 1 mg/mL. After resuspension the solutions were vigorously vortexed until cloudy after which they would undergo bath sonication for 30 minutes at a constant temperature of 60 °C. The lipid vesicle solutions were then extruded through the desired polycarbonate thin film filter (30 nm, 100 nm, and 200 nm) to produce small unilamellar vesicles

of uniform size. All lipid vesicles suspensions were stored at 4 °C and used within 2 days of preparation to ensure consistent vesicle structure.

Fabrication of Surface Plasmon Resonance Sensor Chips:

Fabrication of the SPR sensor chips was performed following a previous procedure published by our group.⁸ After the glass microchips were cleaned in piranha solution (**CAUTION!**) 2 nm of chromium (0.5 Å/s) followed by 48 nm of gold (2.0 Å/s), were deposited on to the cleaned glass slides via electron beam physical vapor deposition (EBPVD) (Temescal, Berkeley, CA). The slides were then removed from the EBPVD so that 1-3 nm of SiO₂ could be added onto the gold layer via plasma enhanced chemical vapor deposition (PECVD) using a Unaxis Plasmatherm 790 system (Santa Clara, CA).

Fluorescence Recovery After Photobleaching:

Fluorescence microscopy and bleaching images were acquired on an inverted Leica TCS SP5 II scanning confocal microscope following a previous procedure we published. 40, 41 For both the SLB and curved membrane mimics a 2 % molar ratio of NBD-PE lipids were incorporated into lipid vesicle. Fluorescently labeled lipids were incorporated into either the underlying lipid membrane or attached vesicles to ensure that fluorescent signal was only attributable to one lipid layer at a time. Excitation and bleaching of the NBD labeled lipids was achieved with an argon laser (488 nm). Recovery images were taken every second with 2-line averaging using the LAS AF software package. The images were then processed in ImageJ. The intensity values were used to calculate fractional recovery following a method demonstrated by Axelrod et al. 42

SPR Analysis:

A NanoSPR5–321 (NanoSPR, Chicago, IL), a dual-channel SPR spectrometer with a GaAs semiconductor laser light source set at a wavelength of 670 nm, was used for all SPR biosensing measurements. $^{7, 16, 40, 43, 44}$ The device utilizes a prism with refractive index of n=1.61 and a 30 μ L flow cell. PBS (phosphate buffered saline) running buffer at a pH of 7.4 was used in all experiments with a flow speed of 5 mL/hr.

Nano Tracking Analysis:

Lipid vesicle suspensions of 100 nm and 200 nm were diluted from the stock solution of 1 mg/mL down to 10 μ g/mL. 30 nm lipid vesicle suspensions were diluted down to a concentration of 500 μ g/mL due to presence of high background noise at 10 μ g/mL during the NTA experiments. Analysis of the vesicles was conducted on a NanoSight NS300 with a flow rate of 5 mL/hr.

Statistical Analysis:

Principal component analysis (PCA) was accomplished with the prcomp function in R and visualized through the ggbiplot package with an ellipse probability set to 95 % using the collected endpoint data with a total set of over 240 data points. Analysis of variance (ANOVA) was conducted in Excel with the Analysis ToolPak add-in and used the same end point data utilized in PCA. All of the utilized data was found to be statistically relevant.

Monte Carlo Lipid Models:

Monte Carlo methods were utilized to model vesicles with varying ganglioside compositions and to predict their distribution and distance between randomly distributed gangliosides. The simulation was conducted with a home-built R script. The minimum distance between individual gangliosides within the model was calculated and iterated to achieve a dataset of over 30,000 lipid distances. The equations used for these calculations were from the R package "rgl"⁴⁵, which was also used for 3D visualization of the ganglioside distribution.

RESULTS AND DISCUSSION:

Formulation and Characterizations of Curved Membrane Mimics:

Curved membrane mimics offer unique platforms for investigation of complex biophysical interactions.⁴⁶ However, their construction on a solid substrate and the subsequent application in SPR based methods have been very limited to date.^{16, 21-24} We report a straightforward approach here in which the membrane construction process can be traced in real time. Figure 2 shows the sensorgram for the generation of the interface by SPR, accompanied with cartoon illustrations for each construction step.

The formation of the curved biomimetic membrane started with the creation of a SLB composed of 5 % DGS-Ni-NTA and 95 % POPC on a silicated gold surface. This percent DGS-Ni-NTA was selected for effective capture of histidine tagged proteins.^{6, 47} The surface was then saturated with 10 μg/mL of histidine tagged cholera toxin (his-CT) to ensure the anchoring of the protein layer. His-CT acts as the support between the SLB and the ganglioside containing vesicles for their strong binding affinity with the ganglioside GM₁,⁴⁸ and sizable cross reactivity with other gangliosides.⁴⁹ Structurally, these gangliosides differ in their respective head groups by the number of sialic acids present: GA₁ has no sialic acids, GM₁ has one, GT_{1b} has three, and GQ_{1b} has four.^{7, 49-51} The final step was to inject 100 nm lipid vesicles containing 1 % GM₁ and 99 % POPC, creating a curved membrane layer above the SLB.

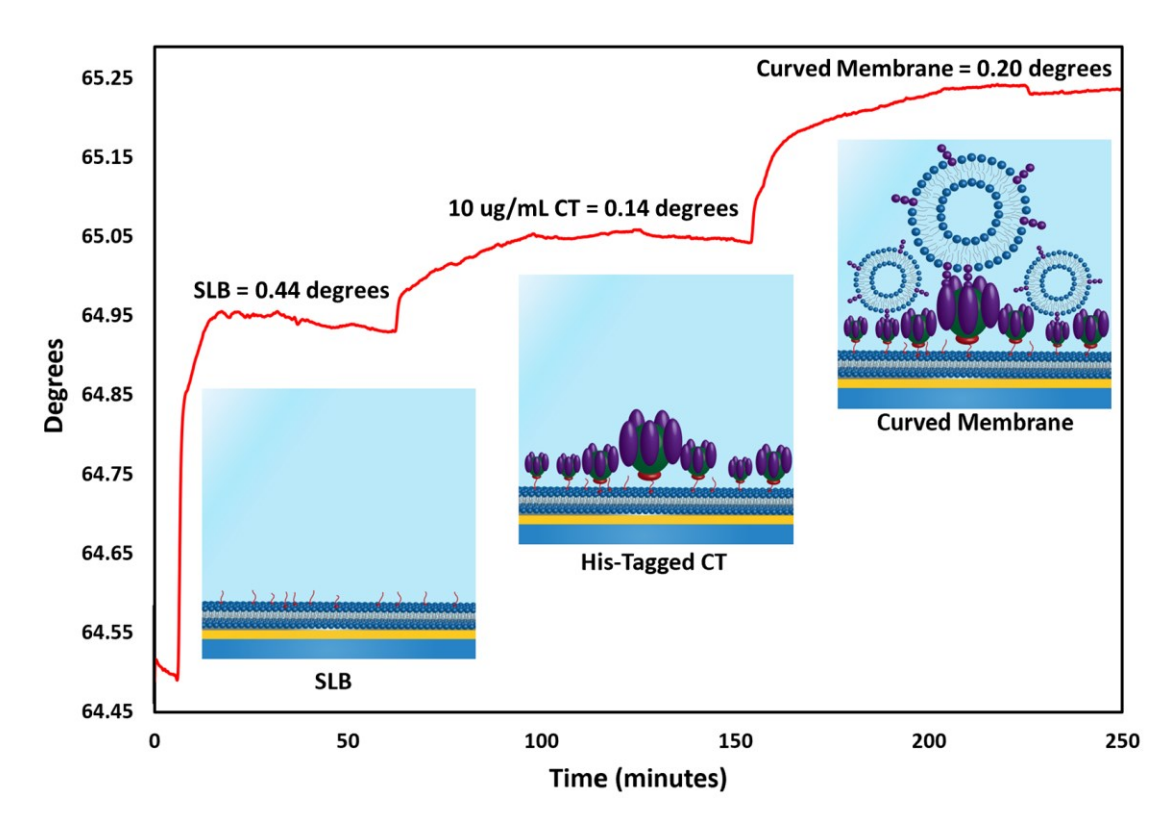


Figure 2. The SPR sensorgram showing the formation of 100 nm 1 % GM1 curved membrane mimic with a cartoon illustration for each step marked in the sensorgram. From left to right is the formation of the DGS-Ni-NTA and POPC SLB, attachment of his-CT as the capture layer, and attachment of the $GM_1/POPC$ vesicles.

As shown in Figure 2, the attachment of vesicle created an angular shift roughly half of that compared to the SLB shift. This led to the question of whether the tethered vesicles remain intact or have fused to form a second SLB on top of the his-CT layer. To probe the form of the

attached vesicles, FRAP was used to determine the fluidity and diffusion properties of the membrane, as shown in Figure 3.

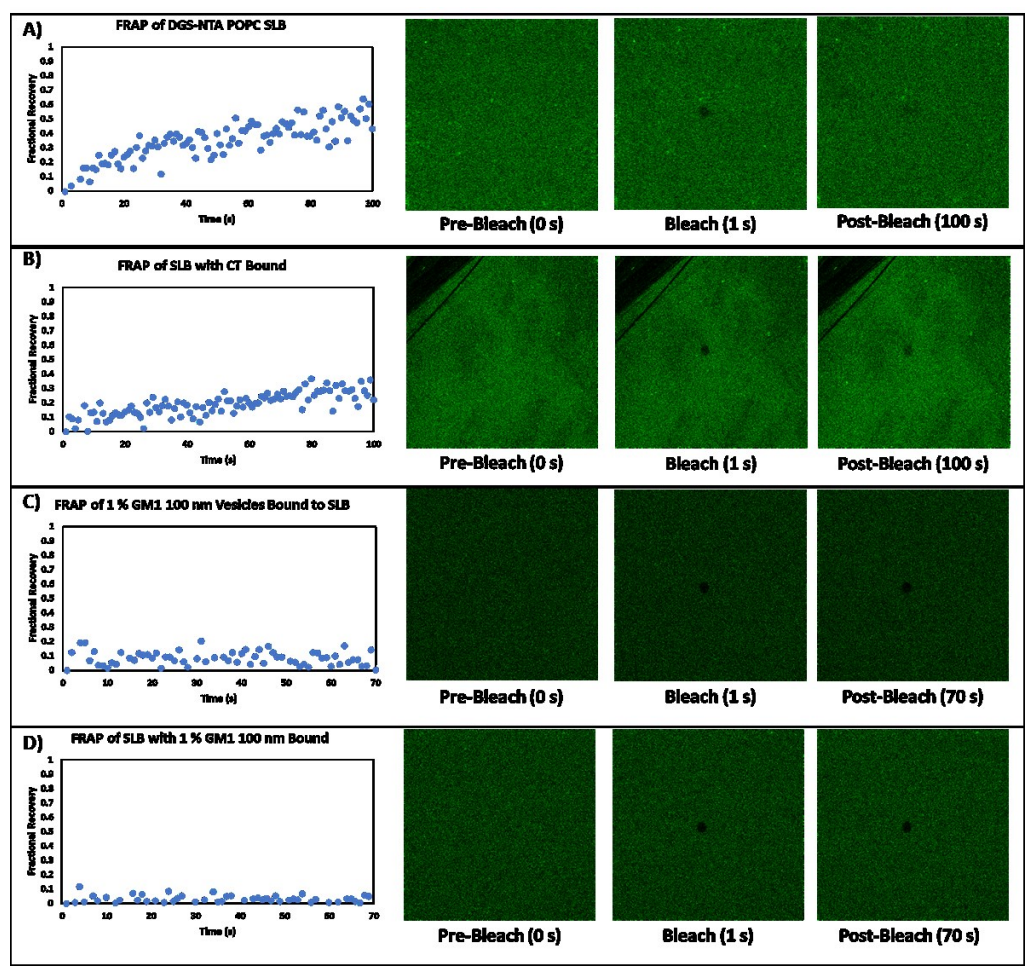


Figure 3. Fluorescence recovery after photobleaching (FRAP) results of A) SLB composed of 5 % DGS-Ni-NTA, 2 % NBD-PE, and 93 % POPC (SLB step in Figure 2), B) SLB composed of 5 % DGS-Ni-NTA, 2 % NBD-PE, and 93 % POPC with 10 μg/mL of his-CT bound to the DGS-Ni-NTA, C) 1 % GM₁, 2 % NBD-PE (his-CT step in Figure 2), and 97 % POPC 100 nm lipid vesicle onto of the SLB with his-CT present (tethered vesicles perspective at curved membrane step in Figure 2), and D) SLB composed of 5 % DGS-Ni-NTA, 2 % NBD-PE, and 93 % POPC with both 10 μg/mL of his-CT and 1 % GM₁ ganglioside 99 % 100 nm lipid vesicle bound (SLB perspective at curved membrane step in Figure 2). For FRAP images of C) and D) fluorophores were incorporated into only the vesicle or solid supported membrane portions respectively.

Figure 3A shows the FRAP of a fluidic SLB. The fluidic membrane obtained substantial recovery over a period of 100s. However, the mobile fraction is substantially lower than that for a purely POPC membrane, which can be attributed to the presence of 5 % DGS-Ni-NTA. This is consistent to literature reports that inclusion of large moieties like DGS-Ni-NTA,⁴⁷ GM₁,⁵² and proteins⁵³ can reduce the mobility of SLB. For comparison, FRAP analysis of a POPC only SLB

can be found in Supporting Figure S3. After his-CT is attached (Figure 3B), a substantial amount of the SLB's fluidity is lost, likely due to the binding that reduced mobility and his-CT's extra mass. Figure 3C showcases the FRAP of the 1 % GM₁, 2 % NBD-PE, and 97 % POPC 100 nm vesicles attached to the his-CT functionalized SLB, indicating that there is no fluidity. This lack of fluidity indicates that the tethered vesicles retained intact and kept their curvature, and did not fuse to form a second SLB. Tethered vesicle fusion usually requires a fusogenic agent such as PEG or Ca²⁺, which are purposely absent in our work. The packing density of the vesicles could be low to support vesicle merging. Figure 3D shows the FRAP study on the underlying SLB with the his-CT and tethered vesicle present. Clearly, the SLB has lost all fluidity and is unable to recover, which agrees with what has been reported in literature. All FRAP results suggest that the his-CT protein layer impedes vesicle rupture and merging, resulting in a stable curved membrane mimicking platform.

Combined results from Figure 2 and Figure 3 indicate that a stable and reliable curved membrane biomimetic platform has been created with tethered vesicles on the CT layer. We next moved to study the impact of the composition and size of the vesicles on biophysical interactions that require curvature. With the curvature and varied degree of gangliosides imbedded, it becomes feasible to probe if the his-CT binding proceeds via a single point or multi-point fashion. The vesicles of sizes of 30 nm, 100 nm, and 200 nm were extruded, and incorporated by different gangliosides at varying percentages ranging between 0.05 % to 5 %, while keeping the SLB composition and amount of his-CT constant.

Curved Membrane Platform Expansion and Capability Evaluation:

We first confirmed that the polycarbonate thin films can reliably generate vesicles of the consistent size batch to batch (Supporting Figure S1) by nano tracking analysis (NTA). The reproducibility of the extruded vesicles for 30 nm, 100 nm, and 200 nm vesicles was high. An average of three batches, each of which underwent three NTA examinations per experiment, were used to report the average size of the vesicles. The results agree well with what has been reported in literature. ^{16, 21}

The percentage of DGS-Ni-NTA in the SLB and the concentration of his-CT were optimized. Based upon a total of 255 experiments it was found that 5 % DGS-Ni-NTA containing

SLB had an average SPR shift of 0.45 degrees with a standard deviation (STD) of 0.01. For 10 μg/mL his-CT an average SPR shift of 0.16 degrees with a STD of 0.02 degrees was observed. GA₁, GM₁, GT_{1b}, and GQ_{1b} gangliosides were incorporated into the 30 nm, 100 nm, and 200 nm vesicles at percentages of 0.05 %, 0.1 %, 1 %, and 5 %. These gangliosides are of importance to the diseases associated with the central nervous system.³⁸

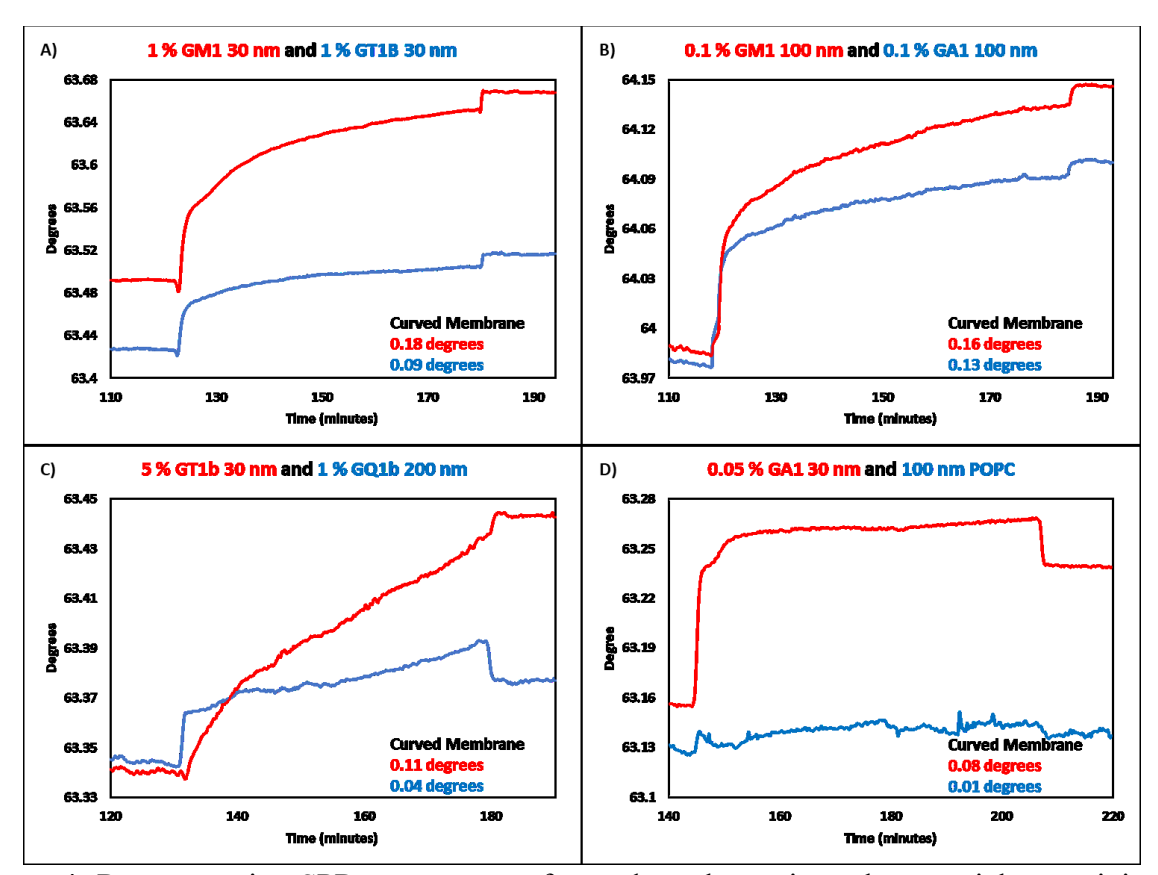


Figure 4. Representative SPR sensorgrams focused on the region where vesicles are injected, incubated, and rinsed A) 1 % GM₁ 30 nm in red and 1 % GT_{1b} 30 nm in blue, B) 0.1 % GM₁ 100 nm in red and 0.1 % GA₁ 100 nm in blue, C) 5 % GT_{1b} 30 nm in red and 1 % GQ_{1b} 200 nm in blue, and D) 0.05 % GA₁ 30 nm in red and 100 nm POPC vesicles in blue.

Figure 4 shows the results of SPR studies on how changing the vesicles composition and size affect the binding kinetics on his-CT layer. Comparing 5 % GT_{1b} 30 nm vesicles (Figure 4C, red) and 1 % GM₁ 30 nm vesicle (Figure 4A, red), the ganglioside present in the vesicles can be more significant than having a higher percentage of a ganglioside with known weaker binding affinity. As shown in Figure 4B, 0.1 % GM₁ 100 nm vesicle (red) and 0.1 % GA₁ 100 nm vesicle (blue), even when utilizing gangliosides known to have highly similar binding kinetics with CT a notable difference between the two can be observed. These trends agree well with what has been

reported in literature on both SLB and SAM, ^{48, 49, 54, 55} but is the first with curved membranes. While the majority of the observed binding interactions can be attributed to the type of ganglioside present, ^{48, 49, 54, 55} it is possible that other factors may be influencing the observations, such as vesicle size and multiple ganglioside interactions.

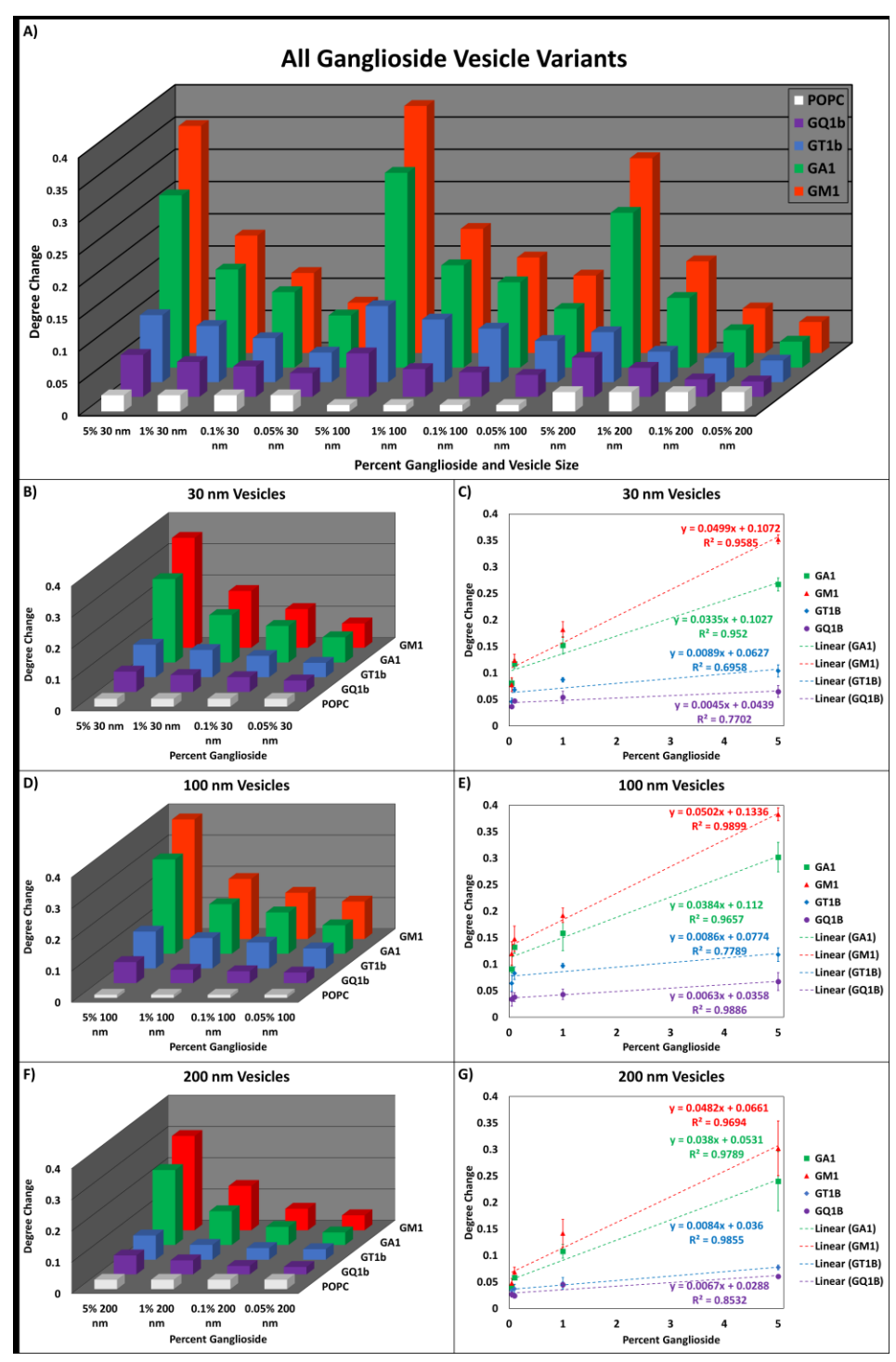


Figure 5. A) 3D bar graph showcasing the overall end point data of all investigated interactions white bars are for lipid vesicles containing only POPC, purple is for all GQ_{1b} ganglioside containing lipid vesicles, blue is for all GT_{1b} ganglioside containing lipid vesicle, green is all GA₁ ganglioside containing vesicles, and red is for all GM₁ containing ganglioside vesicles. The 3D bar graphs of B), D), and F) show the individual end point data values for 30 nm, 100 nm, and 200 nm respectively. Scotter plots for C) 30 nm, E) 100 nm, and G) 200 nm represent the linear trends

observed for each of the investigated gangliosides at that specific vesicles size at increasing percentages based upon the end point data.

To determine the factors besides binding affinities that influence the biophysical interactions, plots of end point data as a 3D bar graph were generated (Figure 5A). We found that the 100 nm vesicles had the largest observable SPR shifts, 30 nm vesicles had the second largest shifts, and 200 nm vesicles had the smallest shifts for all ganglioside types and at each percentage. As SPR's sensitivity depends on changes in mass and refractive index, it can be assumed that the observed changes from the vesicle sizes can mostly be attributed to varying masses.⁴ Because the amount of DGS-Ni-NTA and his-CT were held constant, the number of vesicles that could be tethered should remain constant. Thus, the difference between 100 nm and 30 nm vesicles can be assumed to be mostly dependent on the alteration in mass per area between the two. For the 200 nm vesicles a substantial loss in sensitivity and an increase in variation was observed and several factors were considered as likely explanations for the observed trends. First, the 200 nm tethered vesicles on top of the SLB and his-CT protein layer likely results in the curved membrane mimics being in the outer verge of the 300 nm detection range of the SPR evanescent wave.⁷⁻⁹ Second, the larger size of the 200 nm vesicles may cause greater variation due to the higher malleability of these vesicles. Third, difference in packing density of the vesicles may limit the amount of vesicles that can be captured thus reducing the SPR signal.⁵⁶ Based upon these observations we concluded that the 200 nm tethered vesicles may not be reliably used for SPR biosensing applications.

Separating Figure 5A into respective components based upon vesicle size, we obtained 3D plots for 30 nm (Figure 5 B and C), 100 nm (Figure 5 D and E), and 200 nm (Figure 5 F and G) vesicles to evaluate the trend within each size, which allowed studying the effect of the percentage on vesicle size. It appears that as the head group of the ganglioside differ from GM₁'s, a steady loss in binding affinity can be observed. This trend agrees well with what was previously discussed regarding modifications to the head group of gangliosides binding to CT.^{49, 55}

From Figure 5, there is a positive linear trend between percent ganglioside and SPR shifts for all of the investigated vesicle sizes. However, GT_{1b} and GQ_{1b} containing vesicles show little change for the SPR signals, which can be attributed to their weaker binding affinities with CT, compared to GM_1 and GA_1 .^{49, 55} The observations related to vesicle size and the percent

ganglioside present suggest that SPR may be capable of determining whether a single or multiple point interactions between CT and gangliosides present are implicated in the interactions.

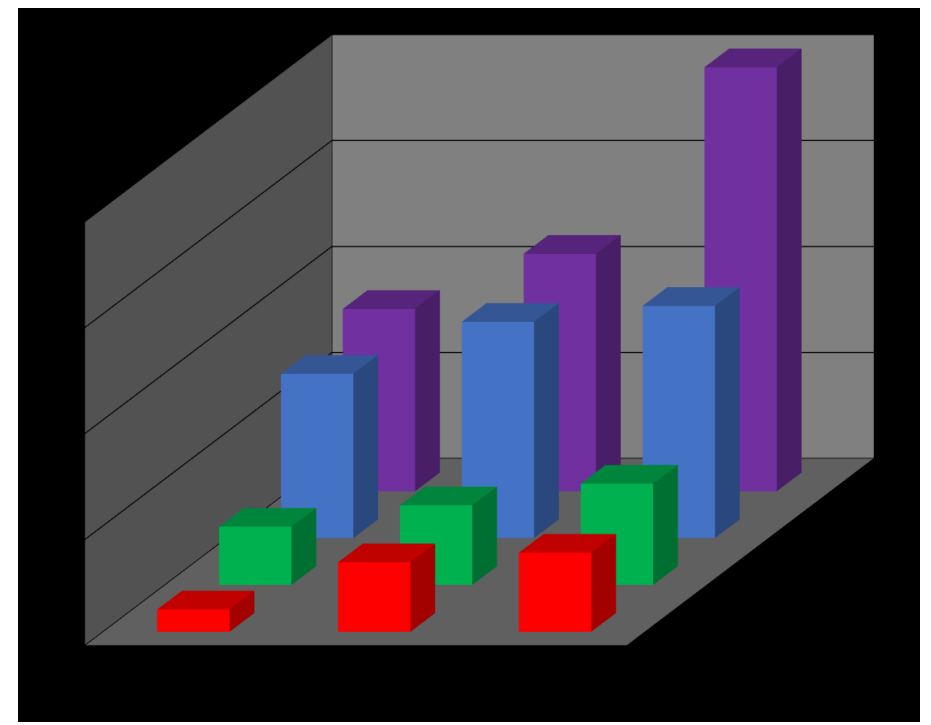


Figure 6. 3D bar graphs showcasing the lowest percentage of ganglioside needed to tether the vesicles for the varying vesicle sizes and compositions (calculated with results in Figure 5). Red is for GM₁, green is for GA₁, blue is for GT_{1B}, and purple for GQ_{1B} for left to right 30 nm, 100 nm, and 200 nm vesicles.

To determine if the interaction to be single point or multi-point interactions, we calculated the lowest percentage for ganglioside needed to tether the vesicles using the extrapolation of the linear relationship. Figure 6 shows the calculated percent limits, via the 3σ method, for each of the investigated gangliosides and vesicle sizes. Based upon the calculated values we found that, for GM₁ containing vesicles, the minimum percent of gangliosides needed for 30 nm vesicles to be detectably tethered was 0.40 %, for 100 nm vesicle was 0.66 %, and for 200 nm vesicles was 0.75 %. For GA₁ the values were 0.55 %, 0.75 %, and 0.96 % for 30 nm, 100 nm, and 200 nm vesicles respectively. GT_{1b} containing vesicles had the values of 1.29 % for 30 nm vesicles, 1.57 % for 100 nm vesicles, and 1.58 % for 200 nm vesicles. For GQ_{1b} containing vesicles the lowest percentages were 1.55 %, 2.61 %, and 3.95 % for 30 nm, 100 nm, and 200 nm vesicles respectively. To predict the interaction mechanism, application of robust post data acquisition analysis tools are needed, as well as taking into account the pentameric structure of CT's B subunit.^{57, 58}

Mathematical Modeling and Statistical Analysis of Vesicle Structure and Biophysical Interactions:

It was hypothesized for systems with values below the lowest percentage can be associated with sing point interactions, and those above the lowest percentage are multi-point interactions.^{59,} ⁶⁰ Additional verification is needed whether the type of ganglioside, percent of ganglioside, or vesicle size were the leading causes of the observed biophysical interactions. To achieve this, several statistical analysis tools were implemented including analysis of variance (ANOVA), principal component analysis (PCA), and Monte Carlo simulations.

PCA was employed to gain a deeper understanding of the significance that the size of the vesicles, ganglioside present, and percent composition of that ganglioside played in the observed biophysical interactions. Before PCA could be performed, data needed to be shown to have no internal bias and were statistically relevant. To prove this, analysis of variance (ANOVA) was applied to the end point data, as shown in Supporting Table S1.

By holding the vesicle sizes constant as shown in Figures 7A, 7B, and 7C for 30 nm, 100 nm, and 200 nm lipid vesicles respectively, the significance of ganglioside species and percentage was revealed. PCA determined that the dominant component for differentiation was the type of ganglioside incorporated into the vesicle, and binding affinities. The percentage of the ganglioside was found to be the most significant factor for the observed misidentification. Minor confusion occurs between GA₁ and GM₁ containing vesicles at percentages of 0.05 % for 30 nm and 100 nm lipid vesicle and below 0.1 % for 200 nm vesicles. GM₁ experienced no confusion with either GT_{1b} nor GQ_{1b} for any sized vesicles. GA₁ and GT_{1b} containing vesicles experienced considerable confusion for 100 nm vesicle below 5 %, though no confusion occurred in 30 nm and 200 nm lipid vesicles. GT_{1b} and GQ_{1b} experienced significant confusion at concentrations below 1 % for 100 nm lipid vesicles, confusion at 0.05 % for 200 nm vesicles, and no confusion at 30 nm vesicles. The observed confusion between the gangliosides and varying percentages can largely be attributed to the high cross reactivity they have with CT. ^{49, 50, 55}

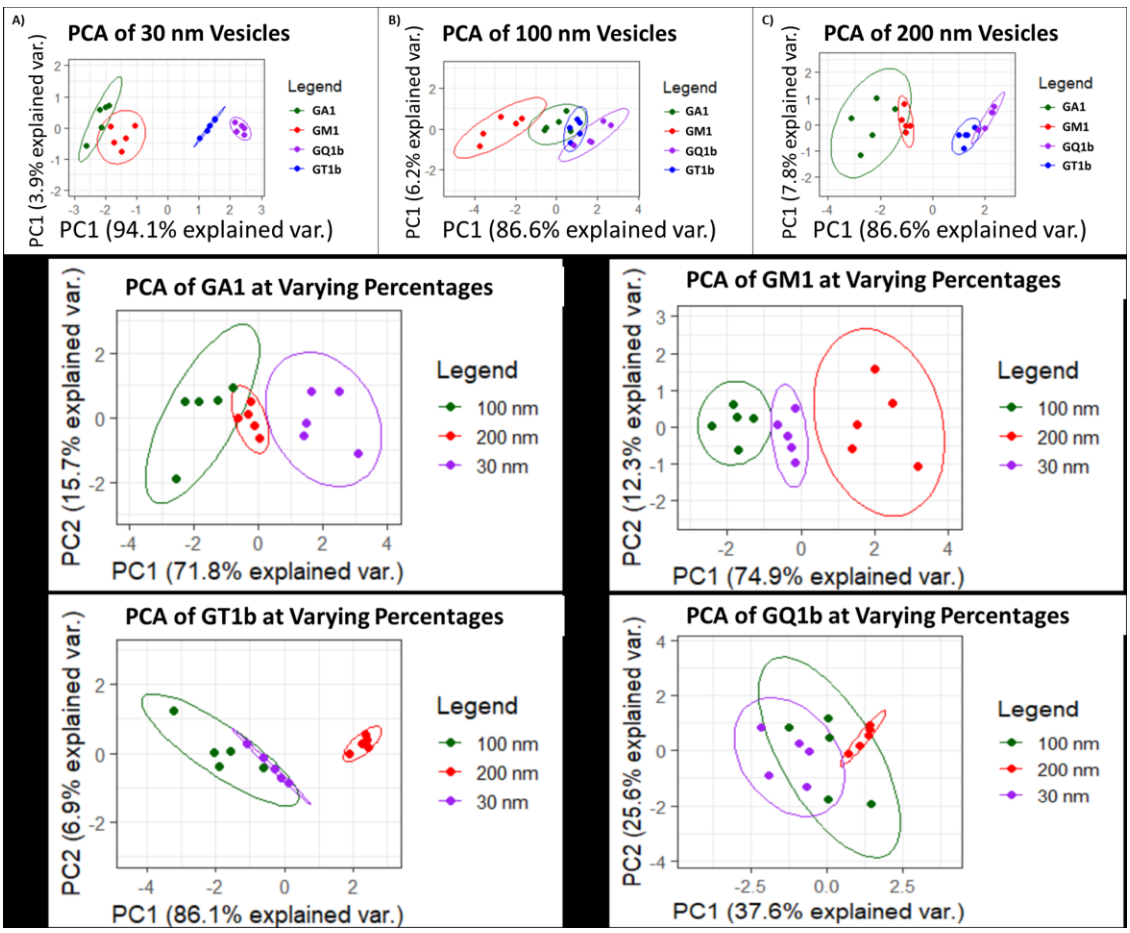


Figure 7. PCA of collected data based upon the control factor for the vesicles where A) is comparing variance based upon 30 nm vesicles and ganglioside present, B) 100 nm vesicles and ganglioside present, and C) 200 nm vesicles and ganglioside present, D) percentage GA₁ ganglioside and size of vesicles, E) percentage of GM₁ ganglioside and size of vesicles, F) percentage of GT_{1b} ganglioside and size of vesicles, and G) percentage of GQ_{1b} ganglioside and size of vesicles.

Figures 7D – 7G for GA₁, GM₁, GT_{1b}, and GQ_{1b} respectively showcase the significance of vesicle size and ganglioside percentage. In this dataset, it was found that the dominant factor was the percentage of that specific ganglioside over the vesicle's size. GA₁ and GM₁ containing vesicles can reliably be differentiated by vesicle size up to 95 % confidence. This is of great interest as it shows that SPR has the potential to be utilized as a new characterization tool for nanostructures functionalized onto a surface, which to date has not been extensively investigated. For GT_{1b} and GQ_{1b} differentiation of the vesicle sizes proved to be considerably difficult for PCA and is most likely due to their substantially weaker binding affinity with CT.^{49, 50, 55} However, as the percentages of GT_{1b} and GQ_{1b} increased differentiation began to be observed, which indicates that their interactions with CT rely heavily on multi-point interactions.

The collected SPR data and PCA results clearly indicated that the most important features, in order of significance, were which ganglioside was present, the percentage of that ganglioside, and the size of the vesicles. However, the importance of ganglioside type and percent ganglioside present, led to the question of whether there was a missing component in the characterization of these biophysical interactions. It became apparent that an evaluation of the statistical likelihood for multi-point or single-point interactions to occur was needed. To determine this required calculating the arc distances for the investigated ganglioside percentage at each vesicles size in a three dimensional (3D) space, while also considering the structure of the antigenic binding domain of CT.

Monte Carlo simulations were carried out to investigate the distribution of the gangliosides in a 3D space. Monte Carlo simulations are essentially a set of algorithms that rely on repeated random sampling techniques to calculate a numerical result of a specific parameter. Monte Carlo methods are most often applied for probability distributions, optimization, or numerical integration. These simulations are useful for building iterative random models that at large scales provide important information about the system in question, especially in the context of spatial distributions. At the context of spatial distributions.

The Monte Carlo simulations used in this study were designed to calculate and compare the arc distances between gangliosides for the investigated ganglioside percentages and vesicles sizes. This approach allowed for the investigation of whether single point or multi-point interactions were occurring between a single vesicle and a captured his-CT. Thousands of vesicles were modeled for each vesicle size and ganglioside percentage, after which each simulation was compiled together to obtain a robust arc length distribution. Using the arc distance distributions and the structure of CT's pentamer GM₁ binding domain an investigation of whether single point or multi-point interactions were occurring could be pursued.

CT is composed of one A subunit and five B subunits. The A subunit of CT is the enzymatic portion of the protein, which has a mass of 28 kDa, and is not present in the his-CT used in the presented study, as it only contains the 5 subunit B portion of CT. The five B subunits, each of which have an individual mass of 11 kDa and a combined mass of 55 kDa, are the receptor binding portions of CT, which has evolved to interact with the sialic acid containing lipid GM₁. ⁵⁷ Recently,

it was reported both through simulations and X-ray crystallography, that CT's pentavalent B subunits are arranged in such a way that they have a 3-nm spacing between one another.⁵⁸ This information was used in combination with the Monte Carlo simulations to determine possible multi-point interactions in binding.

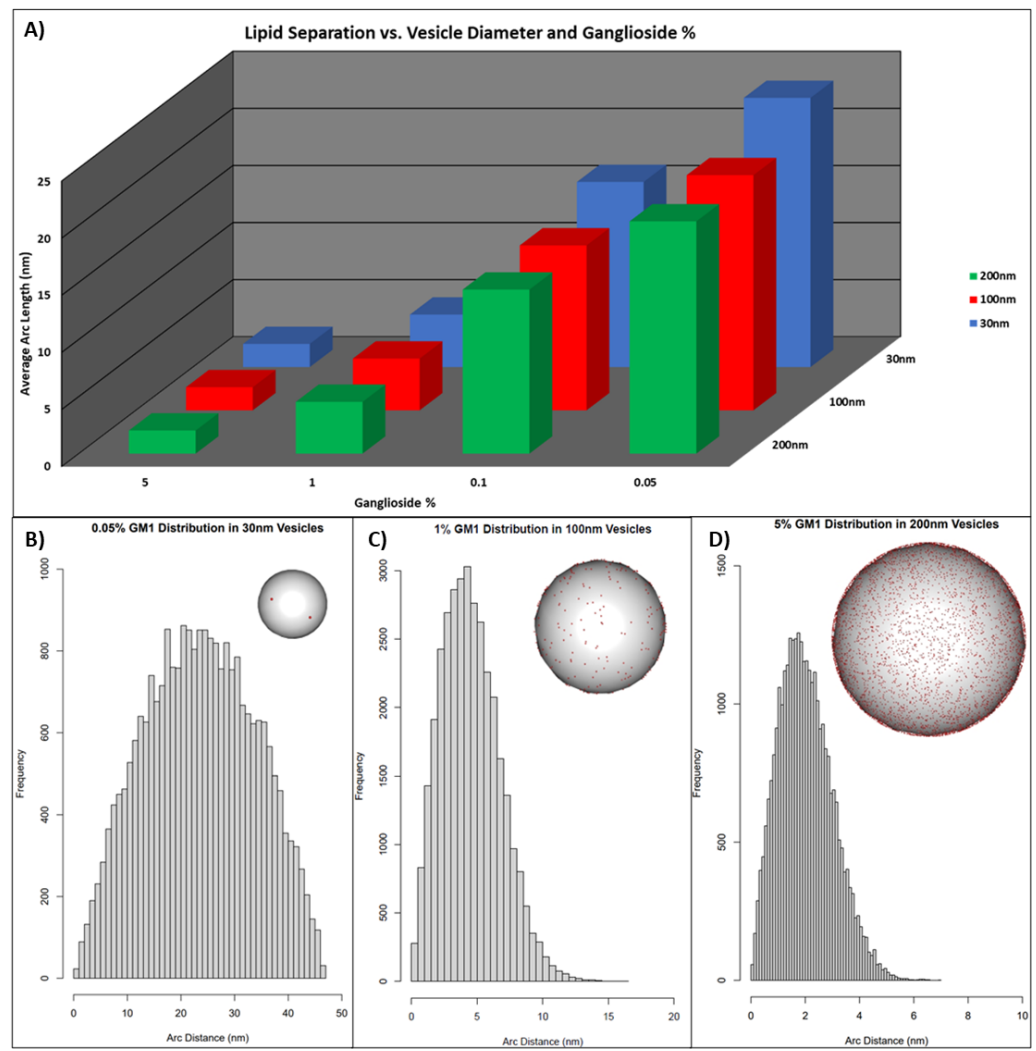


Figure 8. A) Average arc length relation to ganglioside % in each of the three investigated vesicle sizes 30 nm blue, 100 nm red, and 200 nm green, B) example of arc distance of a 0.05 % ganglioside distributed in a 30 nm vesicle, C) arc distance distribution of a 1 % ganglioside distribution in a 100 nm vesicle, and D) example of 5 % ganglioside in a 200 nm vesicle. The red dots indicate the potential location of GM₁ gangliosides in one iteration taken at a specific time point.

With the calculated average arc distances and distribution for every vesicle size and ganglioside percentage investigated in this study, as shown in Figure 8 and the Monte Carlo simulations (Supporting Figure S2), we can determine how the gangliosides present on the surface

of the vesicles would interact with the captured his-CT. The average calculated arc distances for 30 nm lipid vesicles according to the Monte Carlo simulations were 2.03 nm, 4.59 nm, 16.20 nm, and 23.56 nm for 5 %, 1 %, 0.1 %, and 0.05 % respectively. For 100 nm vesicles it was found that the average arc distances were 2.02 nm, 4.53 nm, 14.43 nm, and 20.59 nm at 5 %, 1 %, 0.1 %, and 0.05 % respectively. When 200 nm vesicles were investigated it was found the average arc distances were 2.02 nm, 4.53 nm, 14.16 nm, and 20.33 nm for 5 %, 1 %, 0.1 %, and 0.05 % respectively.

Based upon the collected Monte Carlo data and the assumption that the five B subunits of CT are 3 nm apart it can be inferred that all five of the B subunits would be occupied at 5 % for each of the vesicle sizes. For 1 % ganglioside containing vesicles statistically three to four of the five B subunits would be occupied at every vesicle size. At 0.1 % statistically one to two B subunits could be occupied at any given point, and at 0.05 % it is guaranteed that only single point interactions would be occurring. These results agree well with the proposed lowest percentage calculations for GA₁ and GM₁ to predict whether multi-point or single point interactions were occurring, but did not agree well with the calculated values for GQ_{1b} and GT_{1b} for all vesicles sizes. The observed discrepancy between the Monte Carlo simulations and the calculated values for GQ_{1b} and GT_{1b} at all vesicle sizes can be attributed to the weaker binding affinities with CT.⁵¹ This further indicated the importance of the head group of the molecule being incorporated into the vesicles. Therefore it can be concluded, that the lower binding affinity of GT_{1b} and GQ_{1b} are the dominating factors at play even if multi-point interactions are occurring. This observation agrees well with the observed SPR sensorgrams, shown in Figure 4, and the end point data shown in Figure 5A. In addition to agreeing with the lowest percentage values, the Monte Carlo results agrees well with the PCA's conclusion that the primary cause for the observed biophysical interactions is the percentage of ganglioside over vesicle size.

It can be concluded that the leading biophysical interactions are the binding affinities of the gangliosides and whether or not multi-point interactions are occurring. However, these observations are only true for CT and may be drastically different for other proteins. For this reason, we plan to focus future efforts on investigating known curvature dependent biophysical interactions, such as those affiliated with bridging integrator 1 and alpha-synuclein. ^{15, 18}

Conclusion:

The presented work demonstrated that the combination of SPR with statistical analysis

tools can be a powerful investigation strategy to decipher complex biophysical interactions. In

addition, the creation and characterization of a novel biomimetic curved membrane platform was

presented. The developed platform was shown to be able to reliably generate various curved

membrane mimics in terms of compositions and curvature sizes, while maintaining structural

stability. The combination of this platform and statistics facilitated the identification of whether

single point or multi-point interactions were occurring with his-CT. This platform should facilitate

the investigation of various analyte antigen interactions that rely on curvature but to date have only

been investigated with planar substrates. The information that could be collected from this

platform may drastically aid in the development of new drugs, drug delivery methods, and the

development of new disease detection strategies. Future work will focus on using this platform to

characterize curvature sensing proteins in biological matrices in a manner that has not been pursued

before.

Supporting Information:

Nano tracking analysis of lipid vesicles, cumulative frequency values and arc distances calculated

using Monte Carlo methods, FRAP data for POPC supported lipid membrane, and ANOVA data

for all investigated gangliosides and vesicles sizes (Table S1).

Authors' ORCID ID:

Quan Cheng: 0000-0003-0934-358X

Alex Malinick: 0000-0001-7570-0827

Acknowledgements:

The authors acknowledge supports from NSF (CHE-2109042). We also thank Prof. Wenwan

Zhong for the help with the nano tracking analysis.

References:

- (1) Giacomello, M.; Pyakurel, A.; Glytsou, C.; Scorrano, L. The Cell Biology of Mitochondrial Membrane Dynamics. *Nature reviews Molecular cell biology* **2020**, *21* (4), 204-224.
- (2) De Carvalho, C. C.; Caramujo, M. J. The Various Roles of Fatty Acids. *Molecules* **2018**, *23* (10), 2583.
- (3) Luchini, A.; Vitiello, G. Mimicking the Mammalian Plasma Membrane: An Overview of Lipid Membrane Models for Biophysical Studies. *J Biomimetics* **2020**, *6* (1), 3.
- (4) Hinman, S. S.; McKeating, K. S.; Cheng, Q. Surface Plasmon Resonance: Material and Interface Design for Universal Accessibility. *Analytical chemistry* **2018**, *90* (1), 19.
- (5) Baek, J. M.; Ryu, Y.-S. Surface Sensitive Analysis Device Using Model Membrane and Challenges for Biosensor-Chip. *BioChip Journal* **2020**, *14* (1), 110-123.
- (6) Jackman, J. A.; Cho, N.-J. Supported Lipid Bilayer Formation: Beyond Vesicle Fusion. *Langmuir* **2020**, *36* (6), 1387-1400.
- (7) Malinick, A. S.; Lambert, A. S.; Stuart, D. D.; Li, B.; Puente, E.; Cheng, Q. Detection of Multiple Sclerosis Biomarkers in Serum by Ganglioside Microarrays and Surface Plasmon Resonance Imaging. *ACS sensors* **2020**, *5* (11), 3617-3626.
- (8) Malinick, A. S.; Stuart, D. D.; Lambert, A. S.; Cheng, Q. Surface Plasmon Resonance Imaging (Spri) in Combination with Machine Learning for Microarray Analysis of Multiple Sclerosis Biomarkers in Whole Serum. *Biosensors Bioelectronics: X* **2022**, *10*, 100127.
- (9) Hinman, S. S.; Ruiz, C. J.; Drakakaki, G.; Wilkop, T. E.; Cheng, Q. On-Demand Formation of Supported Lipid Membrane Arrays by Trehalose-Assisted Vesicle Delivery for Spr Imaging. *ACS applied materials Interfaces* **2015**, 7 (31), 17122-17130.
- (10) Hinman, S. S.; Ruiz, C. J.; Drakakaki, G.; Wilkop, T. E.; Cheng, Q. On-Demand Formation of Supported Lipid Membrane Arrays by Trehalose-Assisted Vesicle Delivery for Spr Imaging. *ACS applied materials interfaces* **2015**, *7* (31), 17122-17130.
- (11) Hinman, S. S.; Ruiz, C. J.; Cao, Y.; Ma, M. C.; Tang, J.; Laurini, E.; Posocco, P.; Giorgio, S.; Pricl, S.; Peng, L. Mix and Match: Coassembly of Amphiphilic Dendrimers and Phospholipids Creates Robust, Modular, and Controllable Interfaces. *ACS applied materials interfaces* **2017**, *9* (1), 1029-1035.
- (12) Mazur, F.; Bally, M.; Städler, B.; Chandrawati, R. Liposomes and Lipid Bilayers in Biosensors. *Advances in colloid interface science* **2017**, *249*, 88-99.
- (13) Callan-Jones, A.; Bassereau, P. Curvature-Driven Membrane Lipid and Protein Distribution. *Current Opinion in Solid State Materials Science* **2013**, *17* (4), 143-150.

- (14) Harayama, T.; Riezman, H. Understanding the Diversity of Membrane Lipid Composition. *Nature reviews Molecular cell biology* **2018**, *19* (5), 281-296.
- (15) Oliveira, L.; Gasser, T.; Edwards, R.; Zweckstetter, M.; Melki, R.; Stefanis, L.; Lashuel, H. A.; Sulzer, D.; Vekrellis, K.; Halliday, G. M. Alpha-Synuclein Research: Defining Strategic Moves in the Battle against Parkinson's Disease. *npj Parkinson's Disease* **2021**, *7* (1), 1-23.
- (16) Yang, Z.; Malinick, A. S.; Yang, T.; Cheng, W.; Cheng, Q. Gold Nanoparticle-Coupled Liposomes for Enhanced Plasmonic Biosensing. *Sensors Actuators Reports* **2020**, *2* (1), 100023.
- (17) Simunovic, M.; Evergren, E.; Callan-Jones, A.; Bassereau, P. Curving Cells inside and Out: Roles of Bar Domain Proteins in Membrane Shaping and Its Cellular Implications. *Annual review of cell developmental biology* **2019**, *35*, 111-129.
- (18) Hsieh, W.-T.; Hsu, C.-J.; Capraro, B. R.; Wu, T.; Chen, C.-M.; Yang, S.; Baumgart, T. Curvature Sorting of Peripheral Proteins on Solid-Supported Wavy Membranes. *Langmuir* **2012**, *28* (35), 12838-12843.
- (19) Sundh, M.; Svedhem, S.; Sutherland, D. S. Formation of Supported Lipid Bilayers at Surfaces with Controlled Curvatures: Influence of Lipid Charge. *The Journal of Physical Chemistry B* **2011**, *115* (24), 7838-7848.
- (20) Cawley, J. L.; Jordan, L. R.; Wittenberg, N. J. Detection and Characterization of Vesicular Gangliosides Binding to Myelin-Associated Glycoprotein on Supported Lipid Bilayers. *Analytical Chemistry* **2020**, *93* (2), 1185-1192.
- (21) Park, H.; Sut, T. N.; Yoon, B. K.; Zhdanov, V. P.; Cho, N.-J.; Jackman, J. A. Unraveling How Multivalency Triggers Shape Deformation of Sub-100 Nm Lipid Vesicles. *The Journal of Physical Chemistry Letters* **2021**, *12* (28), 6722-6729.
- (22) Belkilani, M.; Shokouhi, M.; Farre, C.; Chevalier, Y.; Minot, S.; Bessueille, F.; Abdelghani, A.; Jaffrezic-Renault, N.; Chaix, C. Surface Plasmon Resonance Monitoring of Mono-Rhamnolipid Interaction with Phospholipid-Based Liposomes. *Langmuir* **2021**, *37* (26), 7975-7985.
- (23) Norling, K.; Sjöberg, M.; Bally, M.; Zhdanov, V. P.; Parveen, N.; Höök, F. Dissimilar Deformation of Fluid-and Gel-Phase Liposomes Upon Multivalent Interaction with Cell Membrane Mimics Revealed Using Dual-Wavelength Surface Plasmon Resonance. *Langmuir* **2022**, *38* (8), 2550-2560.
- (24) Bompard, J.; Maniti, O.; Aboukhachfe, R.; Ausserre, D.; Girard-Egrot, A. Balm: Watching the Formation of Tethered Bilayer Lipid Membranes with Submicron Lateral Resolution. *Langmuir* **2021**, *37* (31), 9457-9471.
- (25) Black, J. C.; Cheney, P. P.; Campbell, T.; Knowles, M. K. Membrane Curvature Based Lipid Sorting Using a Nanoparticle Patterned Substrate. *Soft Matter* **2014**, *10* (12), 2016-2023.

- (26) Cheney, P. P.; Weisgerber, A. W.; Feuerbach, A. M.; Knowles, M. K. Single Lipid Molecule Dynamics on Supported Lipid Bilayers with Membrane Curvature. *Membranes* **2017**, 7 (1), 15.
- (27) Parthasarathy, R.; Yu, C.-h.; Groves, J. T. Curvature-Modulated Phase Separation in Lipid Bilayer Membranes. *Langmuir* **2006**, *22* (11), 5095-5099.
- (28) Belkilani, M.; Farre, C.; Chevalier, Y.; Minot, S.; Bessueille, F.; Abdelghani, A.; Jaffrezic-Renault, N.; Chaix, C. Mechanisms of Influenza Virus Ha2 Peptide Interaction with Liposomes Studied by Dual-Wavelength Mp-Spr. *ACS Applied Materials Interfaces* **2022**, *14* (29), 32970-32981.
- (29) Bozelli Jr, J. C.; Epand, R. M. Membrane Shape and the Regulation of Biological Processes. *Journal of molecular biology* **2020**, *432* (18), 5124-5136.
- (30) Casares, D.; Escribá, P. V.; Rosselló, C. A. Membrane Lipid Composition: Effect on Membrane and Organelle Structure, Function and Compartmentalization and Therapeutic Avenues. *International journal of molecular sciences* **2019**, *20* (9), 2167.
- (31) Lauwers, E.; Goodchild, R.; Verstreken, P. Membrane Lipids in Presynaptic Function and Disease. *Neuron* **2016**, *90* (1), 11-25.
- (32) Liu, S.; Xiong, X.; Zhao, X.; Yang, X.; Wang, H. F-Bar Family Proteins, Emerging Regulators for Cell Membrane Dynamic Changes—from Structure to Human Diseases. *Journal of hematology oncology* **2015**, δ (1), 1-14.
- (33) Terakawa, M. S.; Lin, Y.; Kinoshita, M.; Kanemura, S.; Itoh, D.; Sugiki, T.; Okumura, M.; Ramamoorthy, A.; Lee, Y.-H. Impact of Membrane Curvature on Amyloid Aggregation. *Biochimica et Biophysica Acta -Biomembranes* **2018**, *1860* (9), 1741-1764.
- (34) Chng, C.-P.; Cho, N.-J.; Hsia, K. J.; Huang, C. Role of Membrane Stretch in Adsorption of Antiviral Peptides onto Lipid Membranes and Membrane Pore Formation. *Langmuir* **2021**, *37* (45), 13390-13398.
- (35) Zhao, M.; Maani, N.; Dowling, J. J. Dynamin 2 (Dnm2) as Cause of, and Modifier for, Human Neuromuscular Disease. *Neurotherapeutics* **2018**, *15*, 966-975.
- (36) Colina-Tenorio, L.; Horten, P.; Pfanner, N.; Rampelt, H. Shaping the Mitochondrial Inner Membrane in Health and Disease. *Journal of Internal Medicine* **2020**, *287* (6), 645-664.
- (37) Pegtel, D. M.; Gould, S. Exosomes. Annual review of biochemistry 2019, 88, 487-514.
- (38) Ledeen, R.; Wu, G. Gangliosides of the Nervous System. *Gangliosides* **2018**, 19-55.
- (39) Cochran Jr, F. B.; Yu, R. K.; Ledeen, R. W. Myelin Gangliosides in Vertebrates. *Journal of neurochemistry* **1982**, *39* (3), 773-779.

- (40) McKeating, K. S.; Hinman, S. S.; Rais, N. A.; Zhou, Z.; Cheng, Q. Antifouling Lipid Membranes over Protein a for Orientation-Controlled Immunosensing in Undiluted Serum and Plasma. *ACS sensors* **2019**, *4* (7), 1774-1782.
- (41) Hinman, S. S.; Ruiz, C. J.; Cao, Y.; Ma, M. C.; Tang, J.; Laurini, E.; Posocco, P.; Giorgio, S.; Pricl, S.; Peng, L.; Cheng, Q. Mix and Match: Coassembly of Amphiphilic Dendrimers and Phospholipids Creates Robust, Modular, and Controllable Interfaces. *ACS applied materials interfaces* **2017**, *9* (1), 1029-1035.
- (42) Axelrod, D.; Koppel, D.; Schlessinger, J.; Elson, E.; Webb, W. W. Mobility Measurement by Analysis of Fluorescence Photobleaching Recovery Kinetics. *Biophysical journal* **1976**, *16* (9), 1055-1069.
- (43) Abouhajar, F.; Chaudhuri, R.; Valiulis, S. N.; Stuart, D. D.; Malinick, A. S.; Xue, M.; Cheng, Q. Label-Free Analysis of Binding and Inhibition of Sars-Cov-19 Spike Proteins to Ace2 Receptor with Ace2-Derived Peptides by Surface Plasmon Resonance. *ACS Applied Bio Materials* **2022**, *6* (1), 182-190.
- (44) Lambert, A. S.; Valiulis, S. N.; Malinick, A. S.; Tanabe, I.; Cheng, Q. Plasmonic Biosensing with Aluminum Thin Films under the Kretschmann Configuration. *Analytical chemistry* **2020**, *92* (13), 8654-8659.
- (45) Rgl: 3d Visualization Using Opengl; 2022. https://CRAN.R-project.org/package=rgl
- (46) Olsén, E.; Jõemetsa, S.; González, A.; Joyce, P.; Zhdanov, V. P.; Midtvedt, D.; Hook, F. Diffusion of Lipid Nanovesicles Bound to a Lipid Membrane Is Associated with the Partial-Slip Boundary Condition. *Nano letters* **2021**, *21* (19), 8503-8509.
- (47) Zou, H.; Wu, J.; Fang, Y. [the Preparation of Supported Lipid Bilayers and Its Functional Study]. *Sheng Wu Yi Xue Gong Cheng Xue Za Zhi* **2019**, *36* (1), 85-93. DOI: 10.7507/1001-5515.201801028.
- (48) Iwamori, M.; Takamizawa, K.; Momoeda, M.; Iwamori, Y.; Taketani, Y. Gangliosides in Human, Cow and Goat Milk, and Their Abilities as to Neutralization of Cholera Toxin and Botulinum Type a Neurotoxin. *Glycoconjugate journal* **2008**, *25* (7), 675-683.
- (49) Kuziemko, G. M.; Stroh, M.; Stevens, R. C. Cholera Toxin Binding Affinity and Specificity for Gangliosides Determined by Surface Plasmon Resonance. *Biochemistry* **1996**, *35* (20), 6375-6384.
- (50) Iwamori, M.; Takamizawa, K.; Momoeda, M.; Iwamori, Y.; Taketani, Y. Gangliosides in Human, Cow and Goat Milk, and Their Abilities as to Neutralization of Cholera Toxin and Botulinum Type a Neurotoxin. *Glycoconjugate journal* **2008**, *25* (7), 675-683.
- (51) Angström, J.; Teneberg, S.; Karlsson, K.-A. Delineation and Comparison of Ganglioside-Binding Epitopes for the Toxins of Vibrio Cholerae, Escherichia Coli, and Clostridium Tetani:

- Evidence for Overlapping Epitopes. *Proceedings of the National Academy of Sciences* **1994**, *91* (25), 11859-11863.
- (52) Goins, B.; Masserini, M.; Barisas, B.; Freire, E. Lateral Diffusion of Ganglioside Gm1 in Phospholipid Bilayer Membranes. *Biophysical journal* **1986**, *49* (4), 849-856.
- (53) Yamazaki, V.; Sirenko, O.; Schafer, R. J.; Groves, J. T. Lipid Mobility and Molecular Binding in Fluid Lipid Membranes. *J Am Chem Soc* **2005**, *127* (9), 2826-2827. DOI: 10.1021/ja0424301.
- (54) Fukuta, S.; Magnani, J. L.; Twiddy, E. M.; Holmes, R. K.; Ginsburg, V. Comparison of the Carbohydrate-Binding Specificities of Cholera Toxin and Escherichia Coli Heat-Labile Enterotoxins Lth-I, Lt-Iia, and Lt-Iib. *Infection immunity* **1988**, *56* (7), 1748-1753.
- (55) Terrettaz, S.; Stora, T.; Duschl, C.; Vogel, H. Protein Binding to Supported Lipid Membranes: Investigation of the Cholera Toxin-Ganglioside Interaction by Simultaneous Impedance Spectroscopy and Surface Plasmon Resonance. *Langmuir* **1993**, *9* (5), 1361-1369.
- (56) Park, H.; Sut, T. N.; Yoon, B. K.; Zhdanov, V. P.; Kim, J. W.; Cho, N.-J.; Jackman, J. A. Multivalency-Induced Shape Deformation of Nanoscale Lipid Vesicles: Size-Dependent Membrane Bending Effects. *The Journal of Physical Chemistry Letters* **2022**, *13* (6), 1480-1488.
- (57) Zhang, R.-G.; Scott, D. L.; Westbrook, M. L.; Nance, S.; Spangler, B. D.; Shipley, G. G.; Westbrook, E. M. The Three-Dimensional Crystal Structure of Cholera Toxin. *Journal of molecular biology* **1995**, *251* (4), 563-573.
- (58) Groza, R.; Ewers, H. Membrane Deformation by the Cholera Toxin Beta Subunit Requires More Than One Binding Site. *Proceedings of the National Academy of Sciences* **2020**, *117* (30), 17467-17469.
- (59) Lauer, S.; Goldstein, B.; Nolan, R. L.; Nolan, J. P. Analysis of Cholera Toxin-Ganglioside Interactions by Flow Cytometry. *Biochemistry* **2002**, *41* (6), 1742-1751.
- (60) Turnbull, W. B.; Precious, B. L.; Homans, S. W. Dissecting the Cholera Toxin—Ganglioside Gm1 Interaction by Isothermal Titration Calorimetry. *J Am Chem Soc* **2004**, *126* (4), 1047-1054.
- (61) Harrison, R. L. Introduction to Monte Carlo Simulation. In *AIP conference proceedings*, 2010; American Institute of Physics: Vol. 1204, pp 17-21.
- (62) Couto, P. R. G.; Damasceno, J. C.; Oliveira, S. d.; Chan, W. Monte Carlo Simulations Applied to Uncertainty in Measurement. *Theory applications of Monte Carlo simulations* **2013**, 27-51.

Graphic Content

